Behavioral/Cognitive

Stabilizing Immature Dendritic Spines in the Auditory Cortex: A Key Mechanism for mTORC1-Mediated Enhancement of Long-Term Fear Memories

Giulia Concina,[1*] Antonia Gurgone,[1*] Elena M. Boggio,[2] Alessandra Raspanti,[1] Riccardo Pizzo,[1] Noemi Morello,[1] Enrico Castroflorio,[1] Tommaso Pizzorusso,[2,3] Benedetto Sacchetti,[1] and Maurizio Giustetto[1]

[1]Department of Neuroscience, University of Turin, Turin, 10125, Italy, [2]Institute of Neuroscience, National Research Council, Pisa, 56124, Italy, and [3]Scuola Normale Superiore, Biology Laboratory BIO@SNS, Pisa, 56124, Italy

Mammalian target of rapamycin (mTOR) pathway has emerged as a key molecular mechanism underlying memory processes. Although mTOR inhibition is known to block memory processes, it remains elusive whether and how an enhancement of mTOR signaling may improve memory processes. Here we found in male mice that the administration of VO-OHpic, an inhibitor of the phosphatase and tensin homolog (PTEN) that negatively modulates AKT-mTOR pathway, enhanced auditory fear memory for days and weeks, while it left short-term memory unchanged. Memory enhancement was associated with a long-lasting increase in immature-type dendritic spines of pyramidal neurons into the auditory cortex. The persistence of spine remodeling over time arose by the interplay between PTEN inhibition and memory processes, as VO-OHpic induced only a transient immature spine growth in the somatosensory cortex, a region not involved in long-term auditory memory. Both the potentiation of fear memories and increase in immature spines were hampered by rapamycin, a selective inhibitor of mTORC1. These data revealed that memory can be potentiated over time by the administration of a selective PTEN inhibitor. In addition to disclosing new information on the cellular mechanisms underlying long-term memory maintenance, our study provides new insights on the molecular processes that aid enhancing memories over time.

Key words: auditory cortex; dendritic spines; learning and memory; mTOR; PTEN; inhibition

---

Significance Statement

The neuronal mechanisms that may help improve the maintenance of long-term memories are still elusive. The inhibition of mammalian-target of rapamycin (mTOR) signaling shows that this pathway plays a crucial role in synaptic plasticity and memory formation. However, whether its activation may strengthen long-term memory storage is unclear. We assessed the consequences of positive modulation of AKT-mTOR pathway obtained by VO-OHpic administration, a phosphatase and tensin homolog inhibitor, on memory retention and underlying synaptic modifications. We found that mTOR activation greatly enhanced memory maintenance for weeks by producing a long-lasting increase of immature-type dendritic spines in pyramidal neurons of the auditory cortex. These results offer new insights on the cellular and molecular mechanisms that can aid enhancing memories over time.

Introduction

Mammalian target of rapamycin (mTOR) and its downstream targets, including ribosomal protein S6 kinase (S6K) and eukaryotic elongation factors 1A and 2 (eEF1A and eEF2), play an important role in synaptic plasticity (Hoeffer and Klann, 2010; Graber et al., 2013; Saxton and Sabatini, 2017). These proteins are mostly involved in the mRNAs recruitment to ribosomes and regulate the initiation and elongation phases of translation (Hay and Sonenberg, 2004; Roux and Topisirovic, 2018). Moreover, S6K integrates signaling from mTOR, phosphoinositide 3-kinases (PI3K), and extracellular signal–regulated kinase (ERK) to modulate protein synthesis. This process starts with the phosphorylation of the ribosomal protein S6 (rpS6), a component of the 40S ribosome, which in turn modulates protein synthesis (Bohlen et al., 2021).

mTOR exists in two distinct complexes, mTORC1 and mTORC2 (Hay and Sonenberg, 2004). The first, which displays sensitivity to rapamycin, promotes different arrays of anabolic processes, and it is linked to both transcriptional and translational machinery. mTORC2 acts via rapamycin-insensitive mechanisms and promotes cell survival in response to growth factors stimulation and stress (Jacinto et al., 2006; Shiota et al., 2006; Zhou and Huang, 2010). The importance of mTORC1 for learning and memory was revealed by showing that rapamycin-induced inhibition of mTORC1 blocks long-term memory (MacCallum et al., 2014; Garza-Lombó and Gonsebatt, 2016).

In accordance with these data, fear learning triggers an increase in mTORC1 activity and the phosphorylation of S6K1 in mice (Sun et al., 2016; Switon et al., 2017; Koehl et al., 2021), while mice carrying mutations of downstream targets of mTORC1 (i.e., 4E-BP2, S6K1, and S6K2) show abnormal long-term memory (Costa-Mattioli et al., 2009). Also, the mTORC2-mediated control of actin polymerization has been linked to long-term memory (Huang et al., 2013; Zhu et al., 2018). Nevertheless, the cellular mechanisms through which mTORC1 and mTORC2 underlie memory processes are yet to be defined. Moreover, most studies have tested the effects of mTOR blockade on memory processes, while it remains largely unknown whether and how an enhancement of mTOR activity and its downstream targets may improve memory formation. Although several inhibitors of the mTOR pathway are available, very few compounds can enhance its activity. Putative candidates have arisen by studying selective inhibitors of the phosphatase and tensin homolog deleted on chromosome 10 (PTEN), a phosphatase that dephosphorylates phosphatidylinositol (3,4,5)-trisphosphate (PIP_3) counteracting PI3K and resulting in the inhibition of AKT, an upstream positive regulator of mTOR (Rosivatz et al., 2006). The balance between PTEN and PI3K activities determines the cellular levels of PIP_3, which is a critical regulator of the serine/threonine kinase AKT to link growth factor signaling with cellular metabolism and survival (Iwanami et al., 2009). Interestingly, PI3K activation was able to increase the formation of new dendritic spines in cultured hippocampal neurons and improve hippocampal-dependent learning (Enriquez-Barreto et al., 2014). Recent studies showed that the infusion of the water-soluble vanadium-based complex 3-hydroxypicolinate vanadium (VO-OHpic) in mice prevented PTEN-dependent dephosphorylation of PIP_3 (Rosivatz et al., 2006; Mak et al., 2010) and rescued synaptic function and memory dysfunctions in cellular and animal models of Alzheimer's disease (Knafo et al., 2016). Here, we investigated the effects of VO-OHpic treatment in healthy mice to assess whether and how an enhancement of mTOR activity improves memory performance.

Materials and Methods

Animals. All procedures were performed in accordance with the European Community Council Directive 2010/63/UE for care and use of experimental animals with protocols approved by the Italian Minister for Scientific Research (Authorization #175/2015-PR) and the Bioethics Committee of the University of Torino. Animal suffering was minimized, as was the number of animals used. Mice were bred in the internal facility of the Department of Neuroscience. After weaning, mice were housed 4 per cage on a 12 h light/dark cycle (lights on at 7:00 h) in a temperature-controlled environment (21 ± 2°C) with food and water *ad libitum*. For this study, 8- to 9-week-old male C57BL/6J mice were used. Because we did not observe any noticeable interindividual phenotypic or metabolic (e.g., weight and health condition scores) difference among the mouse cohorts used in this study, no inclusion/exclusion criteria were adopted besides age and sex (male) of the animals. Two-photon imaging was performed using 8-week-old male mice carrying the Thy1-GFP transgene (M-line) as in Landi et al. (2011). All analyses were conducted by investigators blinded to both treatment and training of mice.

Drug treatments. The PTEN inhibitor, VO-OHpic, was dissolved in a saline + 10% DMSO solution (vehicle) and administered intraperitoneally at the dose of 10 µg/kg (Mak et al., 2010). Biochemical analyses were conducted 30 min and 6 h after the injection. In behavioral studies, mice were injected intraperitoneally immediately after fear learning. Rapamycin was injected intraperitoneally at the dose of 4.5 mg/kg dissolved in saline + DMSO 10%.

In a group of mice, VO-OHpic 10 µM was directly injected into the dorsal hippocampus. In this case, mice were anesthetized immediately after fear learning, placed on a stereotaxic frame, and VO-OHpic or vehicle solution was delivered bilaterally (1 µl per side) into the dorsal hippocampus (AP −2.3, L ± 1.5, and V −2.0) according to the Franklin and Paxinos atlas (Paxinos and Watson, 2007) at a rate of 0.5 µl/min. The injection needle was left in place for 1 min after infusion to allow for drug diffusion. The correct needle track was verified on Nissl-stained brain coronal sections.

Western blotting. Brain samples (excluding cerebellum and brainstem) were extracted with RIPA lysis buffer (1% Triton X-100, 150 mM sodium chloride, 50 mM Tris-HCl, pH 7.5, protease inhibitors [Roche], 1 mM PMSF, 1 mM sodium vanadate, 1 mM sodium fluoride, 1 mM DTT). Equal amounts of proteins (100 µg) were resolved by reducing SDS-PAGE and transferred to PVDF membrane (Gurgone et al., 2023). Membranes were blocked in a blocking buffer consisting of 5% BSA dissolved in TBST (TBS/0.1% Tween-20) for 1 h at 37°C. The primary antibodies were dissolved in TBST containing 1% BSA, and the blots were incubated at 4°C overnight with constant shaking. The day after, the membranes were incubated with the appropriate secondary antibodies (anti-mouse or anti-rabbit, 1:5000; Sigma) for 1 h at room temperature. The chemiluminescent signal was visualized using Clarity Western ECL Blotting Substrates (Bio-Rad) and analyzed with ImageJ software (National Institutes of Health). For the total protein recognition, the membranes incubated with the phospho-specific antibodies were stripped with stripping buffer containing 2-mercaptoethanol, 1% SDS, and 62.5 mM Tris-HCl, pH 6.8, at 37°C for 30 min and reprobed with the total antibodies. The protein amount was normalized relative to the optical density of vinculin or β-actin; the antibody used to perform the biochemical analyses is reported in Table 1.

DiOlistic labeling and morphologic analysis of dendritic spines. Fluorescence labeling of neuronal structures was performed as we previously described (Arroyo et al., 2014; Meziane et al., 2016). Tefzel tubing (Bio-Rad) was placed on a tubing preparation station (Bio-Rad) and filled with polyvinylpyrrolidone (0.32 mg/ml). 1,1′-Dioctadecyl-3,3,3′,3′-tetramethylindocarbocyanine perchlorate crystals (DiI; Invitrogen) were dissolved in methylene chloride (Supelco) and then gently dropped onto the tungsten particles (1.3 µm in diameter; Bio-Rad). DiI-coated particles were immersed in distilled water, and the solution was vortexed, sonicated, and then immediately injected into the predried tubing. Finally, the particle-coated tube was rotated and air-dried under constant nitrogen flow (0.2 L/min) for 1 h and subsequently cut into small pieces (microcarriers) that were stored in a desiccated environment at room temperature. Mice were anesthetized and perfused with 4% PFA in 0.1 M PB. Brains were postfixed in the same fixative solution, washed several times in PB 0.1 M, and then cut into 300 µm sections on a vibratome (Leica VT 1000S). A commercially available helios gene gun system (Bio-Rad) was used to propel DiI-coated particles into fixed slices. A membrane filter with a 3.0 µm pore size (Millipore) was placed between the gun and the tissue to filter out large clusters of coated particles. The particles were accelerated with a shot of inert helium gas (200 psi), slices were then placed in 4% PFA for 2 h, washed 3 times in 0.1 M PB, and mounted on glass slides. A confocal microscope (LSM-5 Pascal or LSM 900; Zeiss, 191 DE) equipped with a 40× oil-immersion objective was used to acquire images from fluorescently labeled secondary and tertiary branches of dendrites in the L2-3 of somatosensory (S1) and the secondary auditory cortex (Te2).

Table 1. List of antibodies used

| Primary antibody | Species of origin | Working dilution | | Supplier and catalog no. |
		WB	IHC	
p-Akt^{Ser473}	Rabbit	1:1000	—	Cell Signaling and Technology Labs code #9271
Akt	Rabbit	1:1000	—	Cell Signaling and Technology Labs code #4691
p-rpS6$^{Ser240-4}$	Rabbit	1:1000	1:1000	Cell Signaling and Technology Labs code #2215
rpS6	Rabbit	1:1000	—	Cell Signaling and Technology Labs code #2217
p-ERK1/2$^{Thr202/Tyr204}$	Rabbit	1:1000	—	Cell Signaling and Technology Labs code #4370
ERK1/2	Rabbit	1:1000	—	Cell Signaling and Technology Labs code #9194
β-actin	Rabbit	1:1000	—	Cell Signaling and Technology Labs code #4970
BDNF	Rabbit	1:500	—	Santa Cruz Biotechnology code #sc-65514
p-TrkB^{Y816}	Rabbit	1:500	—	Abcam code #ab229908
TrkB	Mouse	1:500	—	Santa Cruz Biotechnology code #sc-7268
EF1α	Mouse	1:2000	—	Millipore code #05–235
Vinculin	Rabbit	1:1000	—	Abcam code #ab219649

For each experimental group, at least 8 neurons per animal, for a total of 3 or 4 animals, were identified by using four coronal sections. From each section, at least 10 Z-stack images spaced 0.5 μm apart were collected to generate the dataset, resulting in at least 1000 spines analyzed per group. Dendritic segments and spines size were analyzed quantitatively with ImageJ software (version 1.34S; National Institutes of Health, public domain). Mean spine density was measured as the number of spines per dendritic length unit (μm), with an independent replicate (animal) used as the sampling unit. Neck-length and head-diameter dimensions were used to calculate neck/head ratios as in Meziane et al. (2016) to identify spine types as follows: mature spines, including mushroom (neck/head ratio $<$ 1.1) and stubby (without a neck) protrusions; immature spine, including thin spines (neck/head ratio $>$ 1.1); and filopodia.

Immunohistochemistry and quantitative analysis. Animals were anesthetized 30 min after vehicle/VO-OHpic treatment, transcardially perfused with 4% PFA, and brains were dissected and kept in the same fixative solution overnight at 4°C. After several washes in 0.1 M PB, the brains were then cryoprotected by immersion in 10%, 20%, and 30% sucrose solutions and subsequently cut into 30 µm sections with a cryostat. Free-floating immunostaining and diaminobenzidine reaction was performed as previously described (Chapleau et al., 2012; Ciccarelli et al., 2013; Amendola et al., 2014; Pizzo et al., 2016). After a blocking step in a PBS solution containing 0.05% Triton X-100 and 10% NGS, sections were then incubated overnight at room temperature with rabbit anti-phospho-rpS6$^{Ser240-4}$ (Table 1) diluted in PBS with 3% NGS and 0.05 Triton X-100. Sections were then washed and incubated for 1 h with goat anti-rabbit biotinylated secondary antibodies (1:250; Vector Labs) diluted in 3% NGS and 0.05% Triton X-100 in PBS and transferred to a solution containing a biotin–avidin complex (1:100, Vector Labs). The peroxidase reaction product was visualized by incubation in a solution containing 3,3'-diaminobenzidine (0.05% in Tris–HCl, pH 7.6) with 0.01% H_2O_2 for 3 min. Sections were mounted on gelatin-coated glass slides.

To evaluate changes of p-rpS6$^{Ser240-4}$ immuno-positive neurons, we acquired images of three nonconsecutive coronal brain sections from 4-6 animals per group that included S1 or Te2 cortices according to a mouse brain atlas (Paxinos and Watson, 2007). A transmitted-light microscope (Eclipse 800, Nikon) equipped with a CCD camera (Axiocam HRc, Zeiss) with a 10× objective (1.0 NA) was used by keeping the bright-field illumination settings constant. A digital box (230.34 μm width) spanning from the pial surface to corpus callosum was superimposed at matched locations on each coronal section of the cerebral cortex. Background values were measured in the corpus callosum, and subtracted from each image using ImageJ software. The total density of p-rpS6$^{Ser240-4}$ immunolabeled cells was manually quantified using the point tool in ImageJ as in Pizzo et al. (2016).

Behavioral procedures. A Skinner box module was used as a conditioning chamber as in previous work (Sacchetti et al., 2002; Grosso et al., 2015). Lateral walls and ceiling were made of stainless steel while the rear and front door were of transparent Plexiglas. The floor was made of stainless-steel rods connected to a shock delivery apparatus. The apparatus was enclosed within a sound-attenuating chamber. Once inside, the animals were left undisturbed for 2 min. After this time, seven auditory stimuli (8 s, 80 dB, 1000 Hz, 22 s intertrial interval) acting as conditional stimulus (CS) were administered by a loudspeaker. The last 1 s of each CS was paired with an unconditional stimulus (US) consisting of a scrambled electric foot shock (intensity, 0.5 mA). Mice were left in the chamber for an additional 1 min, and then returned to the home cage.

Contextual fear memory was tested 48 h after training. Mice were returned to the conditioning chamber and freezing was monitored for 3 min. The mouse behavior was recorded by means of a digital video camera and freezing was measured. Auditory memory retention was tested as short-term memory at 1 h or as long-term memory at 72 h, 2 weeks, and 4 weeks after training, in a totally different apparatus located in a separate experimental room to avoid conditioned fear behavior to contextual cues (Sacchetti et al., 1999; Sacco and Sacchetti, 2010). The apparatus was a 30 cm × 20 cm plastic cage with the floor and the sides walls made of transparent plastic, a grid top on the ceiling and enclosed within a sound-attenuating chamber equipped with an exhaust fan, which eliminated odorized air from the enclosure and provided background noise of 60 dB. Once inside, the subject was left undisturbed for 2 min. After this time, seven CSs were administered identical to those used during conditioning. To test the specificity of auditory memory processes, mice were tested with a novel 15 kHz tone (8s, 75 dB, 15 kHz, 42 s intertrial interval). Freezing response, defined as the complete absence of somatic mobility except for respiratory movements, was taken as a fear index and measured by means of a stopwatch.

Two-photon in vivo imaging. For *in vivo* dendritic spines analyses, control and VO-OHpic-injected male mice were analyzed. Animals were oxygenated and kept warm during both surgery and imaging. Mice were maintained under avertin anesthesia (1 ml/50 mg) and a craniotomy of ∼3 mm of diameter was made (Della Sala et al., 2016) over the primary somatosensory cortex (2 mm posterior from bregma, 2 mm lateral from λ) to obtain an implanted cranial window. The apical dendrites of LV pyramidal neurons in the I – II/III cortical layers were imaged using a custom-built two-photon microscope based on a modified confocal scanhead (Olympus Fluoview) and mode-locked Ti:sapphire laser (Coherent Mira 900) equipped with a 20× water immersion microscope objective (NA = 0.95) at zoom 10 and a resolution of 1024 × 1024 pixels. Two imaging sessions 1 h apart were made before the vehicle or VO-OHpic injection to obtain a baseline of spine dynamic. Then mice received an intraperitoneal injection of VO-OHpic solution or vehicle solution and were allowed to recover in their cages. After 5 h, mice were anesthetized and two further imaging sessions 1 h apart of the dendritic segments previously analyzed were made. To identify the same dendritic segments throughout the whole imaging sessions, low-magnification images were taken to obtain a map of the blood vessels and the dendritic organization in the area of interest.

ImageJ software was used to analyze the imaged dendrites. Twenty-five dendrites for a total of 1.36 mm of length and 31 dendrites for a total

of 1.68 mm of length were considered for control and injected mice, respectively. Each dendritic spine was followed through the imaging sessions and categorized as permanent if present in all the imaging sessions, gained or lost if it appears or disappears, respectively, during the imaging sessions. The turnover ratio was calculated as the number of gained (Ng) or lost (Nl) spines on the total number (Nt) of spines (Ng + Nl)/2Nt. The spine gain and loss fraction were calculated as Ng/Nt and Nl/Nt, respectively (Landi et al., 2011).

Statistical analysis. All data are presented as mean ± SEM. Parametric statistics were used throughout all the experiments. Data from two groups were compared using two-tailed unpaired Student's t tests. Multiple-group comparisons were assessed using two-way ANOVA followed by Fisher's LSD *post hoc* test. Cumulative frequencies of dendritic spine neck/head ratio in treated and untreated animals were compared using the normal distribution Kolmogorov–Smirnov (KS) fitting test. The null hypothesis was rejected at the $p < 0.05$ level. All statistical analyses were performed using Prism software (GraphPad).

Results

VO-OHpic activates AKT/mTOR pathway in mouse cerebral cortex

The PTEN inhibitor VO-OHpic has been described as the most potent and specific molecule that can increase AKT phosphorylation in mouse myocardium (Mak et al., 2010). Here we tested whether intraperitoneal administration of VO-OHpic could affect AKT/mTOR pathway also in the mouse brain. A single injection of VO-OHpic (10 μg/kg, i.p.) rapidly (30 min after injection) activated both AKT/mTOR and ERK1/2 signaling as well as the expression of components of the translational machinery in the forebrain. As shown in Figure 1A, VO-OHpic increased the expression of phospho-rpS6$^{Ser240-4}$ ($t_{(14)} = 5.45$, $p < 0.0001$), phospho-AKT ($t_{(8)} = 2.53$, $p = 0.035$), phospho-ERK ($t_{(8)} = 2.72$, $p = 0.027$), and EF1a ($t_{(13)} = 2.32$, $p = 0.037$), while it did not affect the levels of total rpS6 ($p = 0.07$), AKT ($p = 0.88$), and ERK ($p = 0.27$; vehicle, $n = 7$; VO-OHpic, $n = 8$) proteins.

Because the activation of mTOR pathway is associated with the synthesis of BDNF necessary for activity-dependent synaptic plasticity and memory formation (Takei et al., 2001; Inamura et al., 2005), we evaluated whether PTEN inhibition could trigger the expression of BDNF and the phosphorylation of its receptor, the tyrosine kinase tropomyosin receptor kinase B (TrkB). As shown in Figure 1B, no change was detected 30 min after VO-OHpic injection (BDNF: vehicle vs VO-OHpic $t_{(9)} = 1.93$, $p = 0.086$; pTrkB: vehicle vs VO-OHpic $t_{(9)} = 0.38$, $p = 0.72$ 0.05). Conversely, 6 h after VO-OHpic injection, there was a significant increase in BDNF levels (vehicle vs VO-OHpic $t_{(8)} = 2.51$; $p = 0.036$) and pTrkB (vehicle vs VO-OHpic $T_{(8)} = 3.5$; $p = 0.0081$). No change in total TrkB expression was observed at both time intervals (TrkB 30 min: $T_{(10)} = 0.66$, $p = 0.52$; 6 h: $T_{(16)} = 0.28$, $p = 0.78$; vehicle $n = 7$; VO-OHpic $n = 8$).

VO-OHpic injection affects dendritic spine turnover *in vivo*

Previous studies showed that PTEN ablation modifies dendritic spine density (Skelton et al., 2019). Therefore, to investigate whether and how the inhibition of PTEN through VO-OHpic may interfere with spine organization, we turned to two-photon analysis in the somatosensory cortex (S1) of Thy1-GFP (M line) mice (Fig. 1C) and assessed turnover dynamics. We found that a single injection of VO-OHpic influences spine turnover by reducing the short-term loss, but not the gain, of dendritic spines. As shown in Figure 1D–F, VO-OHpic significantly affected spine turnover ratio (vehicle: pre-injection vs post-injection, $t_{(5)} = 0.78$, $p = 0.46$; VO-OHpic: pre-injection vs

post-injection, $t_{(5)} = 3.92$, $p = 0.011$) without affecting spine gain fraction (vehicle: pre-injection vs post-injection, $t_{(5)} = 1.40$, $p = 0.21$; VO-OHpic: pre-injection vs post-injection, $t_{(5)} = 0.97$, $p = 0.37$) but reducing spine loss (vehicle: pre-injection vs post-injection, $t_{(5)} = 0.15$, $p = 0.88$; VO-OHpic: pre-injection vs post-injection, $t_{(5)} = 7.10$, $p = 0.0009$). Thus, these data show that VO-OHpic can alter dendritic spines dynamics in the cerebral cortex by reducing spine loss briefly after its injection.

VO-OHpic injection during memory consolidation enhances long- but not short-term memory

Our data showed that a single administration of VO-OHpic activates plasticity-relevant signaling pathways and modulated spine remodeling *in vivo*. We thus investigated whether and how this compound may interfere with short- or long-term memory processes. To this aim, mice were trained to associate an acoustic stimulus (a pure tone of 1 kHz, acting as a CS) to an aversive footshock (US). VO-OHpic or vehicle was administered immediately afterward to interfere specifically with the memory consolidation without affecting pain or sensory perception occurring during the acquisition trial (Sacchetti et al., 2002; Zhu et al., 2011; Cambiaghi et al., 2016). Animals were tested 1 h later to test VO-OHpic influence on short-term memory retention. Fear memory was tested by presenting the CSs in a totally new environment to avoid conditioned fear to contextual cues (Sacchetti et al., 2002; Zhu et al., 2011; Cambiaghi et al., 2016). No differences were found between vehicle- and VO-OHpic-injected mice ($t_{(10)} = 0.05$, $p = 0.953$; vehicle $n = 6$, VO-OHpic-injected $n = 6$ mice; Fig. 2A). These data showed that VO-OHpic injection did not affect short-term memory and did not modify freezing behavior per se.

We then investigated the retention of long-term auditory memory by testing animals at 72 h, 2 weeks, and 4 weeks after learning (Fig. 2B). Compared with vehicle-injected mice, in VO-OHpic-injected mice long-term memory was significantly potentiated (2×3 mixed ANOVA, main effect of group $F_{(1,16)} = 9.06$, $p = 0.008$; main effect of time $F_{(2,32)} = 2.78$, $p = 0.077$; group $\times$ time interaction $F_{(2,32)} = 1.77$, $p = 0.186$) at 72 h ($p = 0.003$, vehicle, $n = 9$, VO-OHpic, $n = 10$ mice) and at 2 weeks ($p = 0.021$, vehicle $n = 9$, VO-OHpic $n = 10$), but not at 4 weeks, where there was only a tendency to memory potentiation ($p = 0.173$, vehicle $n = 8$, VO-OHpic $n = 10$; Fig. 2B).

These results pose the question of whether the potentiation of long-term memory induced by VO-OHpic administration arises from a specific enhancement of memory processes or rather to an increment in fear-related processes. To address this, we analyzed the freezing elicited by the presentation of a tone (a 15 kHz tone) never perceived before (Concina et al., 2018, 2021, 2022; Grosso et al., 2018). No differences were detected between the two groups ($t_{(10)} = 1.82$, $p = 0.098$; $n = 6$ mice for both groups; Fig. 2C), thereby suggesting the absence of fear generalization in VO-OHpic-injected mice. These results revealed that the administration of VO-OHpic during memory consolidation improves the maintenance of long-term memory, whereas it leaves unaffected short-term memory and fear generalization processes.

We next assessed whether the administration of VO-OHpic may also improve contextual fear memory. Mice were therefore tested 48 h after learning. Surprisingly, the retention of contextual fear memory was left unchanged by PTEN inhibition ($t_{(10)} = 0.23$, $p = 0.822$, $n = 6$ mice for both groups; Fig. 2D). We also performed an additional experiment by administering VO-OHpic (10 μM) directly into the dorsal hippocampus immediately after
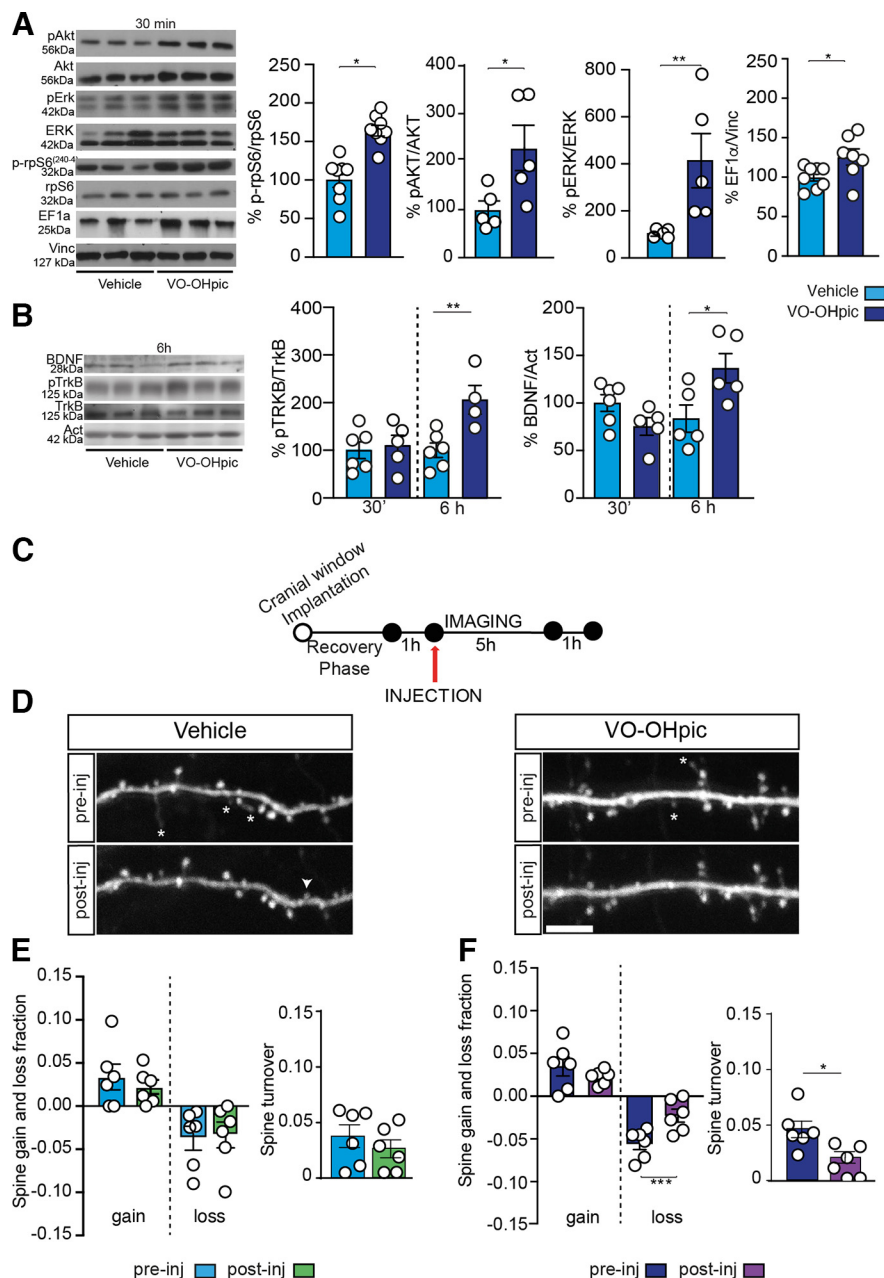
Figure 1. PTEN inhibition with a single injection of VO-OHpic activates AKT/mTOR pathway and affects dendritic spines turnover. **A**, Representative Western blots of PI3K/AKT/mTOR pathway proteins. Quantitative analysis shows that AKT (Ser473), ERK (Thr 202/Tyr204), and rpS6 (SER240-4) phosphorylation as well as EF1α expression significantly increased in mouse forebrain 30 min after VO-OHpic injection. Vinculin was used as loading control. **B**, Representative Western blots of BDNF and pTrkB. Optical density analysis shows that both BDNF and pTrkB expression was unchanged 30 min after VO-OHpic treatment but almost doubled 6 h later. Actin was used as loading control. **C**, Two-photon imaging experimental design. **D**, Images of a dendritic branch from VO-OHpic and vehicle-treated mice before and after the injection. Asterisks indicate lost spines that were lost. Arrowheads point to gained spines through this period. **E**, **F**, VO-OHpic significantly affected spine turnover ratio. PTEN inhibition prevented the loss of immature spines compared (**F**) with vehicle-treated mice (**E**). Data are mean ± SEM. *$p < 0.05$. **$p < 0.01$. ***$p < 0.001$. Scale bar, 5 μm.

learning, and again we found no significant effects on long-term contextual memory ($t_{(6)} = 0.14$, $p = 0.889$; vehicle, $n = 4$; VO-OHpic, $n = 4$; Fig. 2E,F). The latter evidence also supports the idea that VO-OHpic does not enhance basal fear. Combined, our results showed that the administration of VO-OHpic shortly after training elicited a selective long-term potentiation of auditory fear memory.

Changes in dendritic spine morphology underlie the enhancement of long-term auditory fear memory induced by VO-OHpic administration

We next sought to investigate which neural mechanisms triggered by VO-OHpic maintain potentiated fear memories over

time. At first, we tested whether VO-OHpic administration was able to activate the mTOR pathway in the auditory cortex. We analyzed the posterior region of the auditory cortex (i.e., the secondary auditory cortex, Te2), because previous studies showed that this area plays an important role in the long-term maintenance of auditory fear memories (Sacco and Sacchetti, 2010; Grosso et al., 2015; Todd et al., 2018; Concina et al., 2019, 2022; Dalmay et al., 2019). Immunohistochemical analysis showed that, 30 min after VO-OHpic injection, the density of neurons expressing p-rpS6$^{Ser240-4}$ in the Te2 cortex was robustly increased ($t_{(13)} = 2.35$, $p = 0.035$, vehicle, $n = 7$; VO-OHpic, $n = 8$; Fig. 3A,B). Because encoding of long-term memory is linked to a
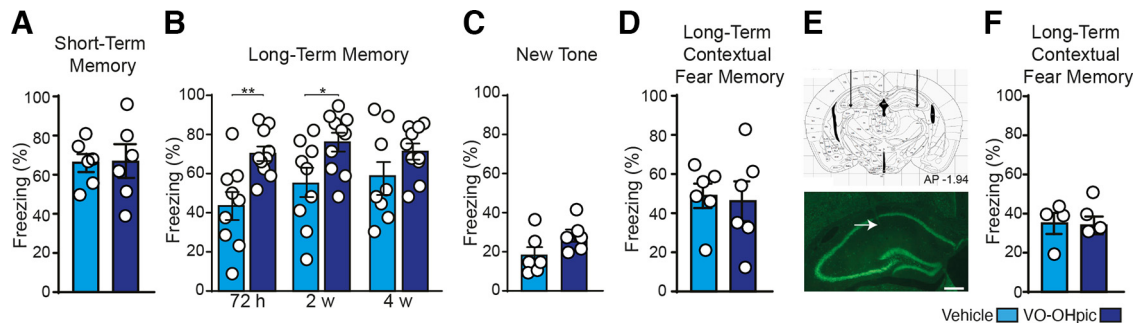
Figure 2. The administration of VO-OHpic during memory consolidation enhances long- but not short-term memory. **A**, VO-OHpic did not affect short-term memory compared with mice receiving vehicle 1 h after conditioning. **B**, Conversely, it significantly increased long-lasting memory at 72 h and 2 weeks, but not at 4 weeks. **C**, No differences were found between mice receiving vehicle or VO-OHpic during the presentation of a new tone 72 h after conditioning. **D**, Vehicle and VO-OHpic-injected mice did not differ from each other in the contextual freezing 48 h after learning. **E**, **F**, Bilateral intrahippocampal infusion of 10 μM VO-OHpic did not affect long-term contextual memory. Left, Arrow indicates a track needle in the dorsal hippocampus. $*p < 0.05$; $**p < 0.01$; Student's t test and 2×3 mixed ANOVA. Data are mean $\pm$ SEM.
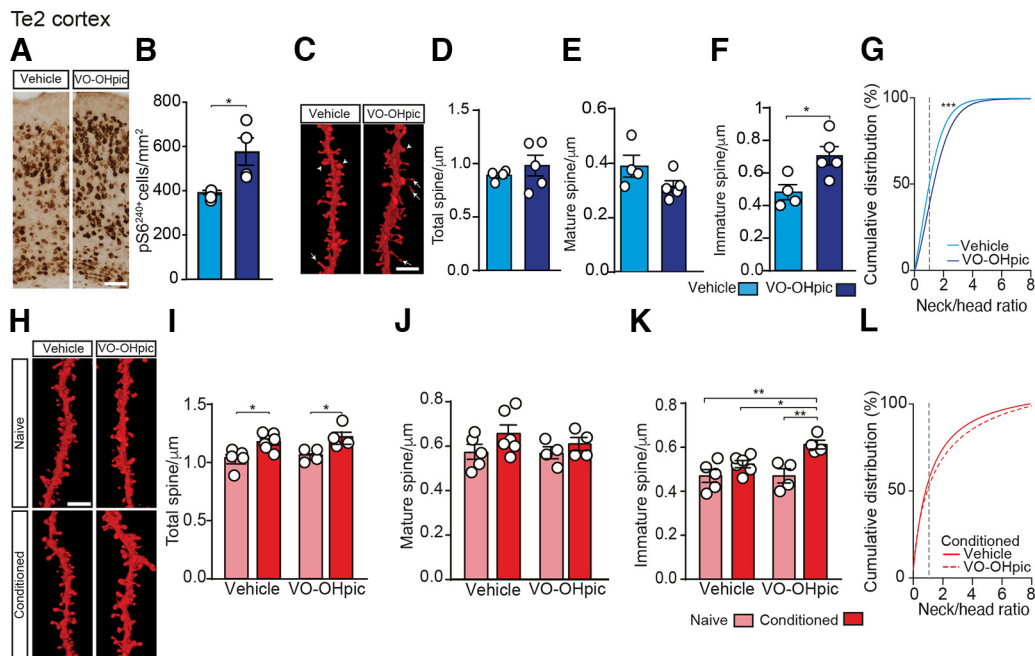

Figure 3. Memory potentiation induced by VO-OHpic injection correlates with a long-term increment of immature dendritic spines in the auditory cortex. **A**, Representative micrographs of Te2 cryosections showing the effect of PTEN inhibition on p-rpS6 (Ser240/244) immunoreactivity 30 min after VO-OHpic injection. Scale bar, 100 μm. **B**, Bar graphs represent rpS6^{240+} cell density 30 min after VO-OHpic injection. **C**, Representative images in Te2 of L2/3 pyramidal neuron dendrites from vehicle- or VO-OHpic-injected mice stained with DiOlistic. Scale bar, 5 μm. Arrows indicate immature spines. Arrowheads indicate mature spines. **D-F**, Total spine density remained unchanged in both vehicle and VO-OHpic conditions. No significant difference was detected in mature spine density (**E**), while immature spines increased after VO-OHpic injection (**F**). **G**, Cumulative analysis of spines distribution based on neck/head ratio. Dotted line indicates immature/mature spine cutoff point. **H**, Representative images of Te2 pyramidal neurons dendrites in naive and conditioned mice. Scale bar, 5 μm. **I**, **K**, Total dendritic spine density was increased 72 h after training in both vehicle- and VO-OHpic- injected mice compared with naive animals. Mature spine density remained unchanged after VO-OHpic injection (**J**), while immature spines were significantly increased (**K**). **L**, Cumulative analysis of spine neck/head ratio. Dotted line indicates immature/mature spine cutoff point. $*p < 0.05$; $**p < 0.01$; $***p < 0.001$; Student's t test, two-way ANOVA, and Fisher's LSD *post hoc* test and KS fitting test. Data are mean $\pm$ SEM.

rearrangement of synaptic contacts and dendritic spines turnover in several brain regions (De Roo et al., 2008; Ruediger et al., 2011), including the auditory cortex (Moczulska et al., 2013; Yang et al., 2016), we assessed by DiOlistic labeling whether VO-OHpic can produce spines remodeling in layer 2/3 neurons of the Te2 region (Fig. 3C–G). This analysis revealed that 6 h after injection, VO-OHpic produced a significant increase in the density of immature spines compared with vehicle ($t_{(7)} = 2.93$, $p = 0.021$, Fig. 3F). In contrast, VO-OHpic produced no significant changes in the density of both mature dendritic spines ($t_{(7)} = 1.74$, $p = 0.12$, Fig. 3E) and total spine protrusions (total: $t_{(7)} = 0.82$, $p = 0.435$; Fig. 3D). Moreover, cumulative distribution

of spine density based on neck/head ratio values (Fig. 3G) revealed a rapid (6 h after injection) rightward shift toward thin/long spines in VO-OHpic-treated animals compared with vehicle-treated controls (KS: D = 0.143, $p < 0.0001$).

Next, we analyzed dendritic spine remodeling in layer 2/3 of Te2 at 72 h after training. Both density and morphology of dendritic spines were analyzed after DiOlistic labeling in the Te2 of conditioned or naive mice injected with vehicle or VO-OHpic (Fig. 3H–L). In vehicle-injected groups, the persistence of fear memories was associated with a significant increase of spine density in conditioned animals ($n = 6$) compared with naive ($n = 5$) animals (two-way ANOVA, group $F_{(1,15)} = 15.88$, $p = 0.001$,
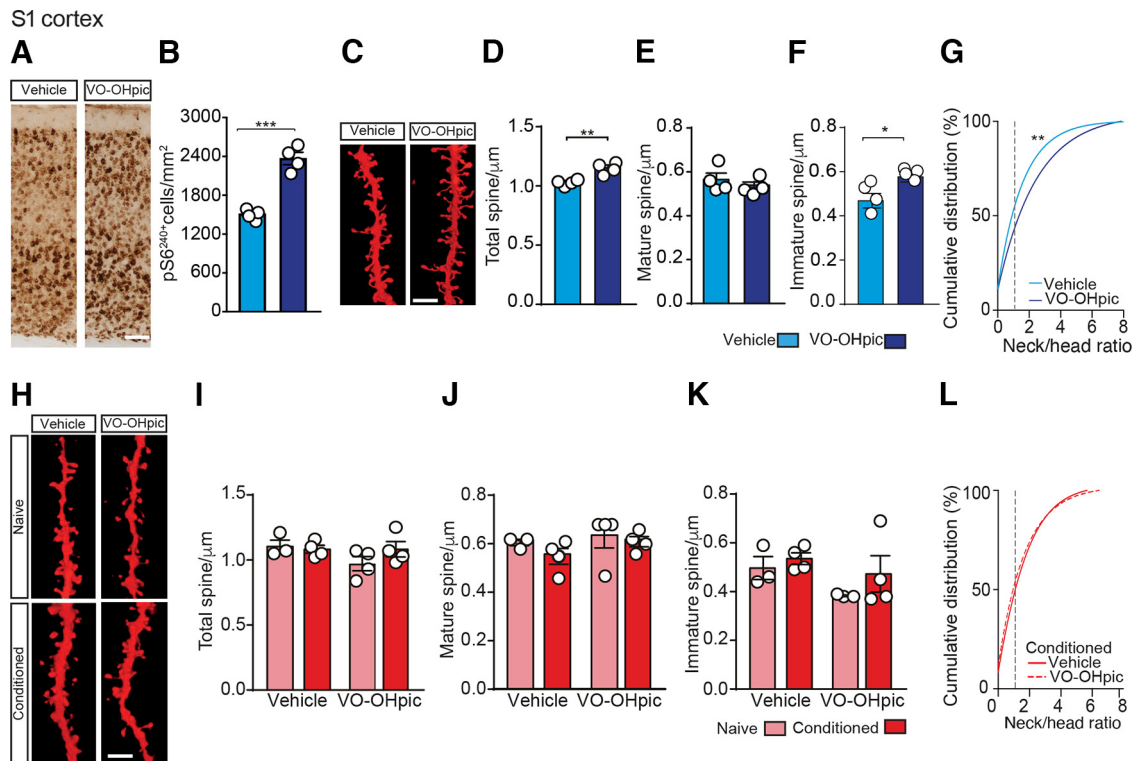
Figure 4. VO-OHpic effects on dendritic spine morphology in the primary somatosensory cortex. *A*, Representative micrographs of S1 cryosections showing the effect of PTEN inhibition on p-rpS6 (Ser240/244) immunoreactivity 30 min after VO-OHpic injection. Scale bar, 100 μm. *B*, Bar graphs represent rpS6^{240+} cell density increase in S1 of treated animals. *C*, Representative images of pyramidal neuron dendrites in S1 from vehicle- or VO-OHpic-injected mice stained with DiOlistic. Scale bar, 5 μm. *D-F*, Bar graphs represent that, 6 h after PTEN inhibition, the density of both total (*D*) and immature spines was significantly increased (*F*), while mature spines remained unaffected (*E*). *G*, Cumulative analysis of spine neck/head ratio. Dotted line indicates immature/mature spine cutoff point. *H*, Representative S1 cortical dendrites stained with DiOlistic. Scale bar, 5 μm. *I-K*, No significant differences in spine density and morphology were detected 72 h after training. *L*, Cumulative analysis of spine neck/head ratio. Dotted line indicates immature/mature spine cutoff point. *p < 0.05; **p < 0.01; ***p < 0.001; Student's *t* test, two-way ANOVA, and Fisher's LSD *post hoc* test and KS fitting test. Data are mean ± SEM.

followed by Fisher's LSD *post hoc*, conditioned-vehicle versus naive-vehicle, p = 0.011; Fig. 3H,I). Similarly, in VO-OHpic-injected groups, conditioned mice (n = 4) showed a greater number of spines compared with naive mice (n = 4; p = 0.013; Fig. 3H,I). Moreover, the number of spines in naive mice injected with VO-OHpic was similar to that of naive mice that received the vehicle (p = 0.680). Thus, VO-OHpic by itself (i.e., in the absence of an associative learning process) did not elicit a persistent change in spine density. Surprisingly, there was no difference of spine density in conditioned mice that received the vehicle and in conditioned mice that received VO-OHpic (p = 0.430; Fig. 3I). The latter result raises the question of whether and how dendritic spine plasticity may be involved in the potentiation of long-term memory detected in VO-OHpic-injected conditioned mice. We therefore analyzed again mature or immature spines separately. Critically, no differences were detected among groups with regard to mature spines (two-way ANOVA, p = 0.094; Fig. 3J), while there was a selective increase in the number of immature spines in conditioned mice injected with VO-OHpic with respect to those which received vehicle (two-way ANOVA, group $F_{(1,15)}$ = 15.73, p = 0.001, followed by Fisher's LSD, p = 0.019; Fig. 3K). VO-OHpic-injected conditioned mice also differed from naive mice that received vehicle (p = 0.001) and naive mice that received VO-OHpic (p = 0.001; Fig. 3K). Interestingly, cumulative distribution of spine neck/head ratio shows a clear, although not statistically significant (KS: D = 0.105, p = 0.07; Fig. 3L), rightward shift in VO-OHpic-treated conditioned animals compared with vehicle-treated conditioned mice, indicative of a higher density of filopodia-like protrusions. These

data thus suggest that memory processes elicited an increase in the number of total dendritic spines in the auditory cortex. On the other hand, PTEN inhibition potentiated long-term memory, and this potentiation was associated with a persistent and selective increase of immature spines.

Structural changes arise by the interplay between PTEN inhibition and memory processes
Thin-immature spines are transient highly plastic structures that are thought to maintain structural flexibility, thus accommodating new, recently enhanced, or weakened inputs (Christoffel et al., 2011; Steffens et al., 2021). Our data suggest that this type of spine may be instrumental to maintain potentiated fear memory for a long time. To address this idea, we analyzed dendritic spines in the S1 cortex, an area not involved in long-term auditory fear memory. First, we tested whether PTEN inhibition can activate in the S1 the phosphorylation of rpS6 at Ser 240-4 and spine growth. VO-OHpic injection produced an increase of p-rpS6$^{Ser240-4}$-positive cells in all the layers of S1 30 min after its injection ($t_{(14)}$ = 2.92, p = 0.011, vehicle, n = 7; VO-OHpic, n = 9; Fig. 4A,B) and a subsequent (at 6 h) change in spine number in S1 ($t_{(6)}$ = 4.44, p = 0.004, n = 4 in both groups; Fig. 4C,D). Then, we analyzed spine morphology 6 h after VO-OHpic (or vehicle) injection also in S1 cortex (Fig. 4C–G). Interestingly, it differed between vehicle and VO-OHpic-injected mice as VO-OHpic increased specifically the subpopulation of immature spines ($t_{(6)}$ = 2.69, p = 0.035; Fig. 4F) without affecting the mature spines ($t_{(6)}$ = 0.76, p = 0.471; Fig. 4E). Moreover, the rightward shift of neck/head ratios distribution

curve indicates that VO-OHpic can rapidly (6 h) induce an increase of thin/long dendritic spines also in S1 (KS: D = 0.173, $p = 0.003$, Fig. 4G). Finally, in the same conditioned mice where we detected changes in Te2 dendritic spines after learning, we analyzed dendritic spines in S1 cortex. No significant differences in total spine density were detected 72 h after training in S1 of conditioned mice receiving vehicle ($n = 4$) or VO-OHpic ($n = 4$) compared with naive animals (two-way ANOVA, $p = 0.429$; vehicle, $n = 3$; VO-OHpic, $n = 4$; Fig. 4H–L). Moreover, no differences were detected between conditioned and naive mice in the number of both mature ($p = 0.322$; Fig. 4J) and immature ($p = 0.234$; Fig. 4K) spines. These results are supported by the cumulative distribution data of neck/head ratio as assessed 72 h after training in S1 (KS: D = 0.1, $p = 0.516$; Fig. 4L).

Hence, despite VO-OHpic being able to activate mTOR pathway and induce spine remodeling in S1 shortly after its injection, the persistence of immature spines did not occur at longer time intervals (i.e., at 72 h after injection). These data suggest that the persistence of immature spine observed at long time intervals in Te2 of conditioned mice that received VO-OHpic arose specifically by the interplay between PTEN inhibition and long-term memory processes.

The blockade of mTORC1 activity prevents VO-OHpic-induced memory enhancement as well as structural changes in Te2

Finally, we assessed whether mTORC1 activity is necessary for long-lasting memory potentiation induced by VO-OHpic. At first, we investigated whether VO-OHpic action can be blocked by rapamycin, a selective inhibitor of mTORC1 (Belelovsky et al., 2009; Li et al., 2014). Rapamycin injection abolished the phosphorylation of rpS6$^{Ser240-4}$ (two-way ANOVA, treatment $F_{(1,18)} = 5.99$, $p = 0.02$; vehicle+VO-OHpic vs rapamycin+VO-OHpic: $F_{(18)} = 2.69$, $p = 0.015$), which was similar to control animals (vehicle+vehicle vs rapamycin+VO-OHpic: $F_{(18)} = 0.39$, $p = 0.7$; Fig. 5A,B). Rapamycin treatment produced also an effect on VO-OHpic-induced AKT phosphorylation (two-way ANOVA, interaction $F_{(1,18)} = 8.89$, $p = 0.008$; vehicle+VO-OHpic vs rapamycin+VO-OHpic: $F_{(18)} = 2.50$, $p = 0.022$) that was similar to vehicle-injected animals (vehicle+vehicle vs rapamycin+VO-OHpic: $F_{(18)} = 0.69$, $p > 0.09$; Fig. 5A–C).

We then tested the effect of rapamycin on fear memory consolidation by injecting it after fear learning in vehicle- and VO-OHpic-injected mice. Rapamycin was administered 3 h after learning because a previous study showed that rapamycin infused into the dorsal hippocampus immediately or 180 min but not 540 min after training impairs long-term memory (Jobim et al., 2012). Rapamycin disrupted memory retention in both vehicle ($n = 6$) and VO-OHpic-injected

←

induced phosphorylation of rpS6 (Ser240-4) but did not affect pAKT (Ser473) expression. Vinculin was used as loading control. **D**, Rapamycin disrupted memory retention in both vehicle and VO-OHpic-injected mice at 72 h after learning. **E**, Two weeks later, rapamycin severely disrupted memory recall in both groups. **F**, Representative images of pyramidal neuron dendrites stained with DiOlistic in Te2 from mice that received either vehicle- or VO-OHpic (left) and rapamycin (right) 72 h after training. **G**, Bar graphs represent that rapamycin significantly affected the increase of total number of spines only in VO-OHpic-injected conditioned animals. Rapamycin specifically impaired the growth of immature spines (**I**) and left mature spine density unaffected (**H**). **J**, Cumulative distribution of spine neck/head ratio. Dotted line indicates immature/mature spine cutoff point. Scale bar, 5 µm. *$p < 0.05$; **$p < 0.01$; ***$p < 0.001$; two-way ANOVA and Fisher's LSD *post hoc* and KS fitting test. Data are mean ± SEM.
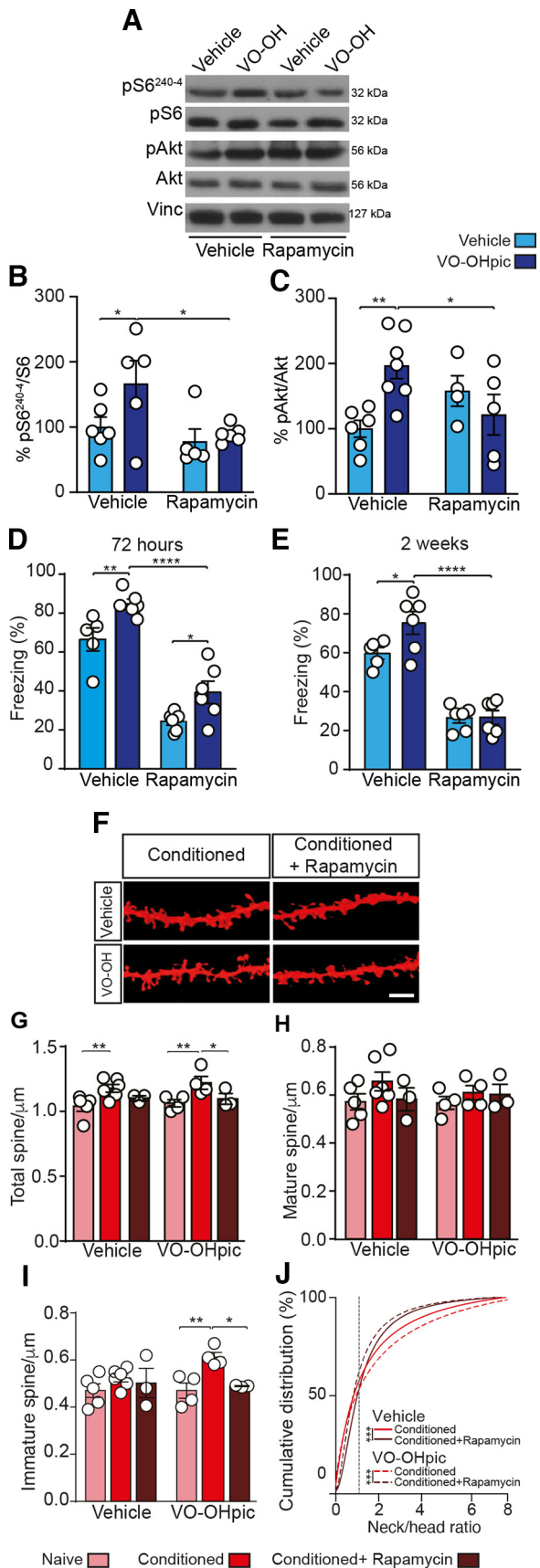
Figure 5. Rapamycin impairs both long-term memory retention and VO-OHpic-induced memory enhancement as well as changes of spine structure. **A**, Representative Western blot of forebrain lysates of mice receiving rapamycin (4.5 mg/kg, i.p.) or vehicle 3 h before PTEN inhibition. **B**, **C**, Western blot quantifications revealed that rapamycin blocked VO-OHpic-

($n = 6$) mice at 72 h (vehicle-vehicle $n = 5$; VO-OHpic-vehicle, $n = 6$; two-way ANOVA, treatment $F_{(1,19)} = 105.05$, $p < 0.0001$; Fig. 5D) and at 2 weeks (treatment $F_{(1,19)} = 101.0$, $p < 0.0001$; Fig. 5E). Seventy-two hours after learning, in mice injected with VO-OHpic and rapamycin, freezing was lower with respect to VO-OHpic-vehicle injected animals ($p < 0.0001$). Interestingly, in VO-OHpic-rapamycin injected mice, freezing was higher than in animals injected with vehicle and rapamycin (VO-OHpic-rapamycin vs vehicle-rapamycin, $p = 0.020$; Fig. 5D), thus suggesting the action of an alternative mechanism to mTORC1. Two weeks later, rapamycin disrupted memory recall in all groups (VO-OHpic-rapamycin vs VO-OHpic-vehicle, $p < 0.0001$; VO-OHpic-rapamycin vs vehicle-rapamycin, $p = 0.962$; Fig. 5E). These results showed that mTORC inhibition affected long-term memory consolidation in control animals, and also hampered memory enhancement in VO-OHpic-injected mice.

We next investigated the effect of rapamycin administration on spines growth and remodeling associated with long-term fear memory (Fig. 5F–J). In conditioned mice that received VO-OHpic and rapamycin ($n = 3$), total spine density was lower with respect to conditioned animals that received VO-OHpic but not rapamycin ($n = 4$) (two-way ANOVA, group $F_{(2,19)} = 9.24$, $p = 0.001$ followed by Fisher's LSD, $p = 0.044$) while it was similar with respect to naive mice that received VO-OHpic ($p = 0.559$; $n = 4$). In mice that did not receive VO-OHpic, rapamycin injection decreased the total spine density in conditioned mice ($n = 3$) at the level of naive animals that did not receive rapamycin ($p = 0.263$; $n = 5$). While rapamycin globally left unaffected mature spines (two-way ANOVA, $p = 0.126$; Fig. 5H), conditioned mice that received both VO-OHpic and rapamycin showed a lower number of immature spines with respect to conditioned animals that received VO-OHpic but not rapamycin (two-way ANOVA, group $F_{(2,19)} = 6.79$, $p = 0.005$ followed by Fisher's LSD, $p = 0.013$; Fig. 5I). Finally, cumulative distribution of neck/head ratios showed that rapamycin prevented the appearance of thin/long spines as illustrated by the significant leftward shift of the frequency curves in both VO-OHpic- and vehicle-treated conditioned animals (vehicle-vehicle vs vehicle-rapamycin KS: D = 0.202, $p < 0.001$; VO-OHpic-vehicle vs VO-OHpic-rapamycin KS: D = 0.215, $p < 0.001$; Fig. 5J). All these data show that mTORC1 activity is needed for the dynamic modifications of dendritic spines associated with memory enhancement obtained by PTEN inhibition.

Discussion

Here we showed that the administration of VO-OHpic, a selective PTEN inhibitor, immediately after learning enhanced long- but not short-term auditory fear memories. This potentiation lasted several weeks and was associated with a long-lasting increase in immature dendritic spine numbers within the auditory cortex. Dendritic spine remodeling was specifically because of the interplay between VO-OHpic and memory processes, as it was absent in S1, a region not involved in auditory fear learning but where VO-OHpic induced spine growth shortly after its injection. Finally, rapamycin, a specific inhibitor of the mTORC1 complex, blocked both memory potentiation and immature spine growth.

In neurons, mTOR complex is present in the postsynaptic compartment, where it is triggered by activity and is critical for synaptic plasticity (Hoeffer and Klann, 2010; Switon et al., 2017). Most of this evidence comes from studies using

pharmacological or genetic inhibition of mTOR pathway. Here we applied a different approach. We investigated the possible effect of an enhancement of AKT/mTOR signaling pathway on dendritic spine remodeling and memory processes. We found that a single injection of VO-OHpic, the most selective and potent PTEN inhibitor (Rosivatz et al., 2006; Mak et al., 2010), rapidly activated AKT in the cerebral cortex; and 6 h after its injection, it also increased spine density on layer 2/3 pyramidal cells in both S1 and Te2 areas. Critically, PTEN inhibition increased specifically the subpopulation of immature spines without affecting the density of mature spines. Indeed, two-photon in vivo imaging analysis of the effect of PTEN inhibition revealed a reduction of spine elimination on layer 5 pyramidal cells in S1. Although it is possible that spines turnover produced by VO-OHpic may not be equivalent in pyramidal cells from different layers (i.e., 2/3 vs 5), our data strongly suggest that PTEN inhibition acts critically on spine dynamics by stabilizing immature spines.

This study has some limitations. Somehow surprisingly, long-term memory enhancement was not associated with changes in spine morphology toward mature spines as suggested for memory storage mechanisms (Bourne and Harris, 2007). This can be because of factors involving the design of the current work and that shall be addressed in the future: specific morphologic changes occurring in a subset of neurons, or spines, that become diluted (and not significant) in our sample; a different stability of immature spines produced by mechanism directly triggered by VO-OHpic enhanced memory; the timing (72 h after training) of spine analyses or the treatment protocol (acute vs chronic); finally, the area of the auditory cortex in which we have focused our analysis (Te2 vs Te1). Previous works reported contrasting results: on one side, PTEN overexpression decreased spine density in the hippocampus while on the other, PTEN knockdown in the BLA decreased total spine density inducing a shifting in the mushroom/thin ratio with an increase of mushroom spines (Haws et al., 2014). In line with our findings, a previous study demonstrated that a peptide which activates the PI3K signaling pathway induced the formation of small, "thin" spines in both hippocampus and cell culture (Enriquez-Barreto et al., 2014). Notably, our results also showed that, in the absence of associative processes, the increase in immature spines induced by PTEN inhibition is a transient process disappearing 72 h after VO-OHpic injection. In contrast, spine remodeling becomes more persistent when it is linked to memory processes, and in this condition, it may enhance long-term memories. Thus, independently from the mechanism of action, our data underscore the importance of the mTOR pathway as a potential druggable target for enhancing learning and memory.

We administered VO-OHpic after learning, and memory retention was tested several days later so that it would act specifically on memory consolidation processes, without interfering either with acquisition or retrieval phases. This allows excluding state-dependent effects and interference with CS and US perception and motor functions (Sacchetti et al., 2002; Cambiaghi et al., 2016). By doing this, we found a selective potentiation of auditory fear memories. In contrast to our findings, a previous study showed that VO-OHpic infusion over a period of 3-4 weeks into brain ventricles did not affect auditory fear memory (Knafo et al., 2016). Despite differences in the type and timing of VO-OHpic administration (a single injection immediately after learning vs prolonged infusion before learning) might account for this discrepancy, future studies should

further address this point. In the same study (Knafo et al., 2016), the prolonged VO-OHpic administration did not modify the retention of long-term contextual fear memory while it rescued normal hippocampal synaptic function and memory dysfunctions in animal models of Alzheimer's disease. Together, with our findings, also showing a lack of effects of a single intrahippocampal injection of VO-OHpic on the long-term contextual fear memory, these data suggest that PTEN modulation may counteract hippocampal synaptic dysfunction and cognitive deficits but not enhance hippocampal-dependent memories in physiological conditions.

Long-term memory potentiation induced by VO-OHpic was accompanied by a selective increment in the number of immature spines in the more posterior region of the auditory cortex, the Te2 cortex, that plays a crucial role in long-term auditory fear memories (Sacco and Sacchetti, 2010; Grosso et al., 2015; Todd et al., 2018; Concina et al., 2019, 2022; Dalmay et al., 2019). In contrast, although 6 h after its injection VO-OHpic produced an increase of immature spines also in S1, an area unrelated to memory consolidation, this increment was no longer present at 72 h in the same animals where spines growth occurred in Te2. We propose that PTEN inhibition and the consequent increase in mTORC activity elicit morphologic changes at the level of dendritic spines. When interacting with memory processes, this determines a persistent increase in immature spines and the strength of enduring memories. The morphology of dendritic spines is a factor influencing spine stability and function and long-lasting changes in synaptic activity are accompanied by alterations in spine shape, size, and number (Hering and Sheng, 2001; Gipson and Olive, 2017; Pchitskaya and Bezprozvanny, 2020). Thin-immature spines are highly plastic structures that respond to synaptic activity underlying learning processes (Gipson and Olive, 2017). These protrusions maintain structural flexibility to enlarge and stabilize (or shrink and dismantle), as they accommodate new inputs (Bourne and Harris, 2007; Lu and Zuo, 2017). Moreover, smaller spines preferentially undergo LTP, whereas larger spines are more stable and show less plasticity. Such observations led to the idea that thin-immature spines represent "plasticity" or "learning" spines (Bourne and Harris, 2007; L. Huang et al., 2020). In this framework, our study showed that a potentiation of long-term memory over time is associated with a persistent increase of immature spines.

mTOR exists in two distinct complexes, mTORC1 and mTORC2 (Kim et al., 2002; McCabe et al., 2020), both of them can be involved in memory processes (Kim et al., 2002; Costa-Mattioli et al., 2009; L. Huang et al., 2020; McCabe et al., 2020). Here we found that memory potentiation produced by VO-OHpic requires mTORC1. VO-OHpic was administered immediately after training allowing the activation of mTOR and BDNF signaling, the latter activating protein translation at dendrites through an mTOR-dependent pathway (Takei et al., 2004). Rapamycin blocked mTORC1 activity 3 h later, probably affecting the second-wave of S6K1 phosphorylation (Garelick et al., 2013; Tee, 2018). In the presence of rapamycin, VO-OHpic-injected mice performed significantly better than vehicle-injected animals at 72 h after learning, thereby suggesting the action of alternative rapamycin-insensitive mechanism(s). However, our data suggest that this mechanism alone (i.e., in the absence of mTORC1 activity) is not sufficient to maintain memory strengthening at more distant time intervals.

In conclusion, our study provides new insights into the molecular mechanisms underlying the maintenance of long-term memories and on the cellular processes that may aid enhancing them. Treatments aimed at counteracting age-related cognitive decline result in an increase in the number of thin spines, suggesting that thin spines are necessary to restore the potential for synaptic plasticity in the aged brain and memory-related diseases (Morrison and Baxter, 2012). Because our study addressed structural modifications in relatively young animals (i.e., 8-9 weeks of age), it will be of paramount interest to investigate in the future whether the modulation of PTEN activity can promote long-term memory enhancement also in older animals, as dendritic spines dynamics in the cerebral cortex profoundly change with aging (Davidson et al., 2020). Moreover, recent studies showed that in schizophrenia patients small spine density is significantly reduced in primary and secondary cortical regions and this may contribute to auditory deficits (Parker and Sweet, 2018). Indeed, individuals with schizophrenia demonstrate auditory hallucinations and deficits in both auditory stimuli processing and auditory memory, which contribute to socio-cognitive dysfunction (Javitt and Sweet, 2015; Kantrowitz et al., 2016; Parker and Sweet, 2018). In this framework, our findings may provide new insights for a novel approach aimed at counteracting small spine reductions and auditory memory dysfunction in schizophrenia.

References

Arroyo AI, Camoletto PG, Morando L, Sassoe-Pognetto M, Giustetto M, Van Veldhoven PP, Schuchman EH, Ledesma MD (2014) Pharmacological reversion of sphingomyelin-induced dendritic spine anomalies in a Niemann Pick disease type A mouse model. EMBO molecular medicine 63:398–413.

Belelovsky K, Kaphzan H, Elkobi A, Rosenblum K (2009) Biphasic activation of the mTOR pathway in the gustatory cortex is correlated with and necessary for taste learning. J Neurosci 29:7424–7431.

Bohlen J, Roiuk M, Teleman AA (2021) Phosphorylation of ribosomal protein S6 differentially affects mRNA translation based on ORF length. Nucleic Acids Res 49:13062–13074.

Bourne J, Harris KM (2007) Do thin spines learn to be mushroom spines that remember? Curr Opin Neurobiol 17:381–386.

Cambiaghi M, Grosso A, Renna A, Sacchetti B (2016) Differential recruitment of auditory cortices in the consolidation of recent auditory fearful memories. J Neurosci 36:8586–8597.

Chapleau CA, Boggio EM, Calfa G, Percy AK, Giustetto M, Pozzo-Miller L (2012) Hippocampal CA1 pyramidal neurons of Mecp2 mutant mice show a dendritic spine phenotype only in the presymptomatic stage. Neural Plast 2012:976164.

Christoffel DJ, Golden SA, Russo SJ (2011) Structural and synaptic plasticity in stress-related disorders. Rev Neurosci 22:535–549.

Ciccarelli A, Calza A, Santoru F, Grasso F, Concas A, Sassoè-Pognetto M, Giustetto M (2013) Morphine withdrawal produces ERK-dependent and ERK-independent epigenetic marks in neurons of the nucleus accumbens and lateral septum. Neuropharmacology 70:168–179.

Concina G, Cambiaghi M, Renna A, Sacchetti B (2018) Coherent activity between the prelimbic and auditory cortex in the slow-gamma band underlies fear discrimination. J Neurosci 38:8313–8328.

Concina G, Renna A, Grosso A, Sacchetti B (2019) The auditory cortex and the emotional valence of sounds. Neurosci Biobehav Rev 98:256–264.

Concina G, Renna A, Milano L, Manassero E, Stabile F, Sacchetti B (2021) Expression of IGF-2 receptor in the auditory cortex improves the precision of recent fear memories and maintains detailed remote fear memories over time. Cereb Cortex 31:5381–5395.

Concina G, Renna A, Grosso A, Sacchetti B (2022) Prior fear learning enables the rapid assimilation of new fear memories directly into cortical networks. PLos Biol 20:e3001789.

Costa-Mattioli M, Sossin WS, Klann E, Sonenberg N (2009) Translational control of long-lasting synaptic plasticity and memory. Neuron 61:10–26.

Dalmay T, Abs E, Poorthuis RB, Hartung J, Pu DL, Onasch S, Lozano YR, Signoret-Genest J, Tovote P, Gjorgjieva J, Letzkus JJ (2019) A critical role for neocortical processing of threat memory. Neuron 104:1180–1194.e7.

Davidson AM, Mejía-Gómez H, Jacobowitz M, Mostany R (2020) Dendritic spine density and dynamics of layer 5 pyramidal neurons of the primary motor cortex are elevated with aging. Cereb Cortex 30:767–777.

Della Sala G, Putignano E, Chelini G, Melani R, Calcagno E, Ratto GM, Amendola E, Gross CT, Giustetto M, Pizzorusso T (2016) Dendritic spine instability in a mouse model of CDKL5 disorder is rescued by insulin-like growth factor 1. Biol Psychiatry 80:302–311.

De Roo M, Klauser P, Garcia PM, Poglia L, Muller D (2008) Spine dynamics and synapse remodeling during LTP and memory processes. Prog Brain Res 169:199–207.

Enriquez-Barreto L, Cuesto G, Dominguez-Iturza N, Gavilán E, Ruano D, Sandi C, Fernández-Ruiz A, Martín-Vázquez G, Herreras O, Morales M (2014) Learning improvement after PI3K activation correlates with de novo formation of functional small spines. Front Mol Neurosci 6:54.

Garelick MG, Mackay VL, Yanagida A, Academia EC, Schreiber KH, Ladiges WC, Kennedy BK (2013) Chronic rapamycin treatment or lack of S6K1 does not reduce ribosome activity in vivo. Cell Cycle 12:2493–2504.

Garza-Lombó C, Gonsebatt ME (2016) Mammalian target of rapamycin: its role in early neural development and in adult and aged brain function. Front Cell Neurosci 10:157.

Gipson CD, Olive MF (2017) Structural and functional plasticity of dendritic spines: root or result of behavior? Genes Brain Behav 16:101–117.

Graber TE, McCamphill PK, Sossin WS (2013) A recollection of mTOR signaling in learning and memory. Learn Mem 20:518–530.

Grosso A, Cambiaghi M, Renna A, Milano L, Merlo RG, Sacco T, Sacchetti B (2015) The higher order auditory cortex is involved in the assignment of affective value to sensory stimuli. Nat Commun 6:8886.

Grosso A, Santoni G, Manassero E, Renna A, Sacchetti B (2018) A neuronal basis for fear discrimination in the lateral amygdala. Nat Commun 9:1214.

Gurgone A, Pizzo R, Raspanti A, Chiantia G, Devi S, Comai D, Morello N, Pilotto F, Gnavi S, Lupori L, Mazziotti R, Sagona G, Putignano E, Nocentini A, Supuran CT, Marcantoni A, Pizzorusso T, Giustetto M (2023) mGluR5 PAMs rescue cortical and behavioural defects in a mouse model of CDKL5 deficiency disorder. Neuropsychopharmacology 48:877–886.

Hay N, Sonenberg N (2004) Upstream and downstream of mTOR. Genes Dev 18:1926–1945.

Haws ME, Jaramillo TC, Espinosa F, Widman AJ, Stuber GD, Sparta DR, Tye KM, Russo SJ, Parada LF, Stavarache M, Kaplitt M, Bonci A, Powell CM (2014) PTEN knockdown alters dendritic spine/protrusion morphology, not density. J Comp Neurol 522:1171–1190.

Hering H, Sheng M (2001) Dendritic spines: structure, dynamics and regulation. Nat Rev Neurosci 2:880–888.

Hoeffer CA, Klann E (2010) mTOR signaling: at the crossroads of plasticity, memory and disease. Trends Neurosci 33:67–75.

Huang L, Zhou H, Chen K, Chen X, Yang G (2020) Learning-dependent dendritic spine plasticity is reduced in the aged mouse cortex. Front Neural Circuits 14:14:581435.

Huang W, Zhu PJ, Zhang S, Zhou H, Stoica L, Galiano M, Krnjević K, Roman G, Costa-Mattioli M (2013) mTORC2 controls actin polymerization required for consolidation of long-term memory. Nat Neurosci 16:441–448.

Inamura N, Nawa H, Takei N (2005) Enhancement of translation elongation in neurons by brain-derived neurotrophic factor: implications for mammalian target of rapamycin signaling. J Neurochem 95:1438–1445.

Iwanami A, Cloughesy TF, Mischel PS (2009) Striking the balance between PTEN and PDK1: it all depends on the cell context. Genes Dev 23:1699–1704.

Jacinto E, Facchinetti V, Liu D, Soto N, Wei S, Jung SY, Huang Q, Qin J, Su B (2006) SIN1/MIP1 maintains Rictor-mTOR complex integrity and regulates Akt phosphorylation and substrate specificity. Cell 127:125–137.

Javitt DC, Sweet RA (2015) Auditory dysfunction in schizophrenia: integrating clinical and basic features. Nat Rev Neurosci 16:535–550.

Jobim PF, Pedroso TR, Werenicz A, Christoff RR, Maurmann N, Reolon GK, Schröder N, Roesler R (2012) Impairment of object recognition memory by rapamycin inhibition of mTOR in the amygdala or hippocampus around the time of learning or reactivation. Behav Brain Res 228:151–158.

Kantrowitz JT, Epstein ML, Beggel O, Rohrig S, Lehrfeld JM, Revheim N, Lehrfeld NP, Reep J, Parker E, Silipo G, Ahissar M, Javitt DC (2016)

Neurophysiological mechanisms of cortical plasticity impairments in schizophrenia and modulation by the NMDA receptor agonist D-serine. Brain 139:3281–3295.

Kim DH, Sarbassov DD, Ali SM, King JE, Latek RR, Erdjument-Bromage H, Tempst P, Sabatini DM (2002) mTOR interacts with raptor to form a nutrient-sensitive complex that signals to the cell growth machinery. Cell 110:163–175.

Knafo S, et al. (2016) PTEN recruitment controls synaptic and cognitive function in Alzheimer's models. Nat Neurosci 19:443–453.

Koehl M, Ladevèze E, Catania C, Cota D, Abrous DN (2021) Inhibition of mTOR signaling by genetic removal of p70 S6 kinase 1 increases anxiety-like behavior in mice. Transl Psychiatry 11:165.

Landi S, Putignano E, Boggio EM, Giustetto M, Pizzorusso T, Ratto GM (2011) The short-time structural plasticity of dendritic spines is altered in a model of Rett syndrome. Sci Rep 1:45.

Li J, Kim SG, Blenis J (2014) Rapamycin: one drug, many effects. Cell Metab 19:373–379.

Lu J, Zuo Y (2017) Clustered structural and functional plasticity of dendritic spines. Brain Res Bull 129:18–22.

MacCallum PE, Hebert M, Adamec RE, Blundell J (2014) Systemic inhibition of mTOR kinase via rapamycin disrupts consolidation and reconsolidation of auditory fear memory. Neurobiol Learn Mem 112:176–185.

McCabe MP, Cullen ER, Barrows CM, Shore AN, Tooke KI, Laprade KA, Stafford JM, Weston MC (2020) Genetic inactivation of mTORC1 or mTORC2 in neurons reveals distinct functions in glutamatergic synaptic transmission. Elife 9:e51440.

Mak LH, Vilar R, Woscholski R (2010) Characterisation of the PTEN inhibitor VO-OHpic. J Chem Biol 3:157–163.

Meziane H, Khelfaoui M, Morello N, Hiba B, Calcagno E, Reibel-Foisset S, Selloum M, Chelly J, Humeau Y, Riet F, Zanni G, Herault Y, Bienvenu T, Giustetto M, Billuart P (2016) Fasudil treatment in adult reverses behavioural changes and brain ventricular enlargement in Oligophrenin-1 mouse model of intellectual disability. Hum Mol Genet 25:2314–2323.

Moczulska KE, Tinter-Thiede J, Peter M, Ushakova L, Wernle T, Bathellier B, Rumpel S (2013) Dynamics of dendritic spines in the mouse auditory cortex during memory formation and memory recall. Proc Natl Acad Sci USA 110:18315–18320.

Morrison JH, Baxter MG (2012) The ageing cortical synapse: hallmarks and implications for cognitive decline. Nat Rev Neurosci 13:240–250.

Parker EM, Sweet RA (2018) Stereological assessments of neuronal pathology in auditory cortex in schizophrenia. Front Neuroanat 11:131.

Paxinos G, Watson C (2007) The rat brain in stereotaxic coordinates. London: Elsevier.

Pchitskaya E, Bezprozvanny I (2020) Dendritic spines shape analysis: classification or clusterization? Perspective. Front Synaptic Neurosci 12:31.

Pizzo R, Gurgone A, Castroflorio E, Amendola E, Gross C, Sassoè-Pognetto M, Giustetto M (2016) Lack of Cdkl5 disrupts the organization of excitatory and inhibitory synapses and parvalbumin interneurons in the primary visual cortex. Front Cell Neurosci 10:261.

Rosivatz E, Matthews JG, McDonald NQ, Mulet X, Ho KK, Lossi N, Schmid AC, Mirabelli M, Pomeranz KM, Erneux C, Lam EW, Vilar R, Woscholski R (2006) A small molecule inhibitor for phosphatase and tensin homologue deleted on chromosome 10 (PTEN). ACS Chem Biol 1:780–790.

Roux PP, Topisirovic I (2018) Signaling pathways involved in the regulation of mRNA translation. Mol Cell Biol 38:e00070-18.

Ruediger S, Vittori C, Bednarek E, Genoud C, Strata P, Sacchetti B, Caroni P (2011) Learning-related feedforward inhibitory connectivity growth required for memory precision. Nature 473:514–518.

Sacchetti B, Lorenzini CA, Baldi E, Tassoni G, Bucherelli C (1999) Auditory thalamus, dorsal hippocampus, basolateral amygdala, and perirhinal cortex role in the consolidation of conditioned freezing to context and to acoustic conditioned stimulus in the rat. J Neurosci 19:9570–9578.

Sacchetti B, Baldi E, Lorenzini CA, Bucherelli C (2002) Cerebellar role in fear-conditioning consolidation. Proc Natl Acad Sci USA 99:8406–8411.

Sacco T, Sacchetti B (2010) Role of secondary sensory cortices in emotional memory storage and retrieval in rats. Science 329:649–656.

Saxton RA, Sabatini DM (2017) mTOR signaling in growth, metabolism, and disease. Cell 168:960–976.

Shiota C, Woo JT, Lindner J, Shelton KD, Magnuson MA (2006) Multiallelic disruption of the Rictor gene in mice reveals that mTOR complex 2 is essential for fetal growth and viability. Dev Cell 11:583–589.

Skelton PD, Frazel PW, Lee D, Suh H, Luikart BW (2019) Pten loss results in inappropriate excitatory connectivity. Mol Psychiatry 24:1627–1640.

Steffens H, Mott AC, Li S, Wegner W, Švehla P, Kan VW, Wolf F, Liebscher S, Willig KI (2021) Stable but not rigid: chronic in vivo STED nanoscopy reveals extensive remodeling of spines, indicating multiple drivers of plasticity. Sci Adv 7:eabf2806.

Sun J, Liu Y, Tran J, O'Neal P, Baudry M, Bi X (2016) mTORC1-S6K1 inhibition or mTORC2 activation improves hippocampal synaptic plasticity and learning in Angelman syndrome mice. Cell Mol Life Sci 73:4303–4314.

Switon K, Kotulska K, Janusz-Kaminska A, Zmorzynska J, Jaworski J (2017) Molecular neurobiology of mTOR. Neuroscience 341:112–153.

Takei N, Kawamura M, Hara K, Yonezawa K, Nawa H (2001) Brain-derived neurotrophic factor enhances neuronal translation by activating multiple initiation processes: comparison with the effects of insulin. J Biol Chem 276:42818–42825.

Takei N, Inamura N, Kawamura M, Namba H, Hara K, Yonezawa K, Nawa H (2004) Brain-derived neurotrophic factor induces mammalian target of rapamycin-dependent local activation of translation machinery and protein synthesis in neuronal dendrites. J Neurosci 24:9760–9769.

Tee AR (2018) The target of rapamycin and mechanisms of cell growth. Int J Mol Sci 19:880.

Todd TP, Jiang MY, DeAngeli NE, Bucci DJ (2018) A functional circuit for the retrieval of remote cued fear memory. Behav Neurosci 132:403–408.

Yang Y, Liu DQ, Huang W, Deng J, Sun Y, Zuo Y, Poo MM (2016) Selective synaptic remodeling of amygdalocortical connections associated with fear memory. Nat Neurosci 19:1348–1355.

Zhou H, Huang S (2010) The complexes of mammalian target of rapamycin. Curr Protein Pept Sci 11:409–424.

Zhu L, Sacco T, Strata P, Sacchetti B (2011) Basolateral amygdala inactivation impairs learning-induced long-term potentiation in the cerebellar cortex. PLoS One 6:e16673.

Zhu PJ, Chen CJ, Mays J, Stoica L, Costa-Mattioli M (2018) mTORC2, but not mTORC1, is required for hippocampal mGluR-LTD and associated behaviors. Nat Neurosci 21:799–802.